

We are IntechOpen, the world's leading publisher of Open Access books Built by scientists, for scientists

6,300

Open access books available

170,000

International authors and editors

185M

Downloads

Our authors are among the

154

Countries delivered to

TOP 1%

most cited scientists

12.2%

Contributors from top 500 universities



WEB OF SCIENCE™

Selection of our books indexed in the Book Citation Index
in Web of Science™ Core Collection (BKCI)

Interested in publishing with us?
Contact book.department@intechopen.com

Numbers displayed above are based on latest data collected.
For more information visit www.intechopen.com



Chapter

Structure and Properties of Biodegradable Polymer Materials for Fused Deposition Modeling 3D Printing

Jing Tian, Yanyan Zheng, Qing Ouyang, Ping Xue, Baohua Guo and Jun Xu

Abstract

The properties of 3D printed products are closely related to the raw materials and the processes by which they are made. The processes of melting, depositing, and cooling of polymers affect the orientation, crystallinity, and microstructure of the product. These in turn influence the thermal, mechanical, optical, and other properties of the printed part. Among various 3D printing methods, filament and pellet extrusion-based fused deposition modeling (FDM) 3D printing is the cheapest and mostly adopted. In this chapter, the devices and some biodegradable polymer materials applicable in FDM 3D printing are briefly introduced. In the first part, preparation and the structure-property relationship of polylactic acid/polybutylene succinate blend filaments are discussed. Rheological, thermal properties of the raw materials and the properties of the printed parts were characterized. In the second part, a pellet extrusion 3D printer with a micro-screw was designed for using pellets of polyhydroxyalkanoate composites, which are difficult to produce filaments. The relationship between the screw parameters of the micro-screw extrusion 3D printer, rheological properties of the composites, and the printed product performance has been investigated. Combining theory and practical application will provide guidance for formulating biodegradable polymer materials and designing equipment for FDM 3D printing.

Keywords: fused deposition modeling, biodegradable polymer materials, structure, rheological properties, mechanical properties

1. Introduction

3D printing, also known as additive manufacturing (AM), refers to a series of processes used to stack into a three-dimensional solid. AM has unique advantages for innovative manufacturing of products owing to its single-piece, low-volume, rapid manufacturing characteristics. AM technology can be classified into different types, such as selective laser melting, selective laser sintering, fused deposition modeling (FDM), etc. Among them, FDM technology is well known for its simplicity and low

cost, which makes FDM unique among the many 3D printing processes. The conditions required during FDM are mild since the plastic has a low melting point and does not produce many harmful substances, allowing for desktop-level printing. The processes that need to be mastered by those operating them are also simple and the final products require little or no post-processing.

Environmental protection, green manufacturing, sustainable economic development, and the search for alternatives to nonrenewable resources have long been issues of global concern. Biodegradable materials derived from renewable sources are the most promising substitutes for petroleum-based resources [1, 2]. The AM of fully biodegradable materials combines the advantages of biodegradable materials and AM technology, therefore, products made of renewable biodegradable materials can be precisely designed and manufactured. FDM technology is the most suitable in AM to process biodegradable composites owing to its wide material compatibility, low cost, and structural design flexibility. This chapter mainly discusses the FDM printing of biodegradable polymer materials and attempts to reveal the relationship between material, equipment, and process parameters, and the performance of printed products, using filament and pellet extrusion FDM as two examples.

2. Filament extrusion 3D printing

2.1 Commonly used filament extrusion 3D printer

Since the commercialization of fused deposition modeling (FDM) 3D printing technology by Stratasys, it has become the most common and fastest-growing 3D printing method, accounting for over 50% of the 3D printing market. Currently, filament extrusion remains the mainstream commercial FDM technology. **Figure 1** shows the principle of FDM-based 3D printing. One of the most common processes today is to take a filament consumable, which must be of a specific diameter (1.75 mm or 3 mm) and is pushed through a pair of filament-feeding gears into a hot melt nozzle for melting. The material extruded from the nozzle is deposited on a three-dimensional

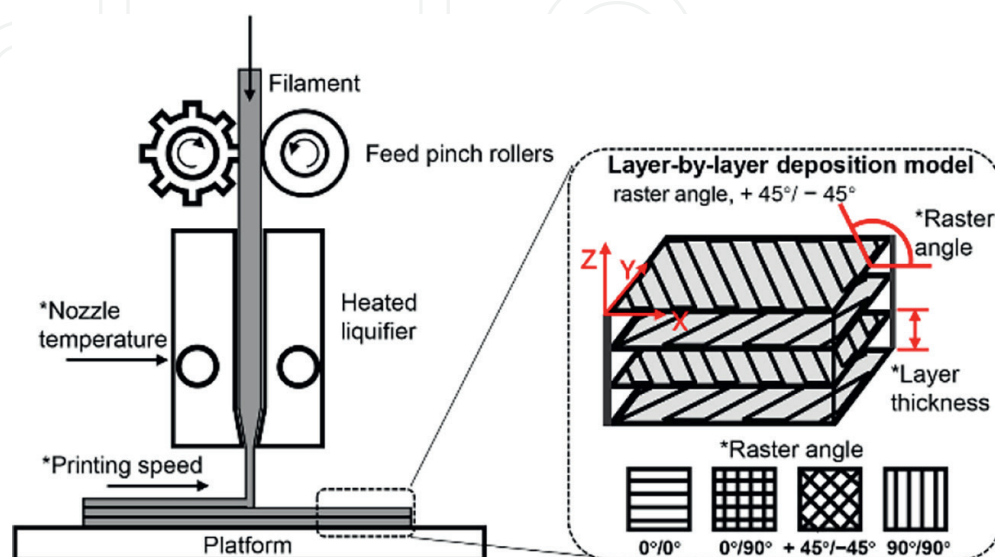


Figure 1.
Principle of FDM-based 3D printing.

platform. The motor drives the nozzle in the X-Y plane and the platform drops one layer in height after each print run, thus achieving layer-by-layer accumulation.

FDM technology is characterized by its simplicity and low cost, however, the quality of the molded part is low and the strength of the interlayer bond is the main factor affecting the mechanical properties. This is owing to the inherent printing principle of FDM technology and the performance of the printed part will vary significantly in different printing directions. This problem is also prevalent in other 3D printing technologies. For the same ABS material, the ultimate stress of an injection molded part was 26 MPa, whereas that of FDM printed bars could only reach a maximum of 22 MPa [3].

The performance of 3D-printed parts is often improved by optimizing the printing parameters. As shown in **Figure 1**, a large number of FDM parameters have different effects on product properties [4]. The effect of different printing parameters on the performance of printed parts has been studied extensively. The main influencing parameters of filament extrusion FDM are raster angle, layer thickness, nozzle diameter, feed rate, infill density, printing speed, etc. The significance of several process parameters in filament extrusion FDM has been reported in the literature: raster angle > layer thickness > printing speed > nozzle temperature [5–18].

2.2 Biodegradable materials commonly used for FDM 3D printing

The widely used biodegradable polymers include polylactic acid (PLA), polyhydroxyalkanoates (PHA), polybutylene succinate (PBS), polybutylene adipate-co-terephthalate (PBAT), and polycaprolactone (PCL), of which PLA, PHA, and some PBS (using fermentation-derived succinic acid) are both bio-based and biodegradable. The biodegradable materials commonly used for FDM are still mainly PLA. There is also a small amount of research on other biodegradable composites, such as PBS, PBAT, and PCL. **Table 1** lists the characteristics of biodegradable polymers commonly used for FDM 3D printing.

Polymer	Printing temperature (°C)	Biodegradation (industrial)*	Biodegradation (ocean)*	Printing characteristics and printed product performance
PLA	190–200	6–9 weeks	>1.5 years	Easier to print and no odor; less warpage; poor heat resistance; and impact resistance
PBS	130–200	2–5 months	>1 year	Heavy warpage; good heat resistance; and toughness
PBAT	150–200	2–3 months	>1 year	Difficult to feed filament; less warpage; good heat resistance, ductility, and impact resistance
PCL	80–100	4–6 weeks	6 weeks	Difficult to feed filament; poor heat resistant
PVA	/	1–2 weeks	4 months	Prone to thermal degradation; commonly used as a water-soluble support material

*Biodegradation refers to industrial compostability under EN 13432 or ASTM D6400 conditions or degradation in ocean water according to the references [2].

Table 1. Characteristics of biodegradable polymers commonly used for FDM 3D printing.

PLA is currently a widely used printing material for home 3D printers. PLA is biodegradable, has no irritating odor, and does not warp easily during the printing process. However, it is less heat resistant, with a glass transition temperature of around 60°C. It is also hard and brittle, with an elongation at break of less than 10% and poor impact resistance, which limits its use in applications requiring ductility and flexibility. Furthermore, PLA biodegrades slowly in the natural environment, mainly through hydrolysis and chain breaking. Overall, PLA biodegradability is dependent on numerous factors such as degradation environment, permeability to water, molecular weight, and crystallinity [19].

PBS is a thermally stable, processable, and biodegradable aliphatic polyester. However, the use of PBS for 3D printing is still relatively unexplored. Because of its low stiffness and high shrinkage, PBS can suffer from severe warpage during printing, leading to print failure, so it needs to be modified before it can be used for filament 3D printing.

To promote the development of FDM-based 3D printing, the design of new environmentally friendly polymeric materials that overcome the disadvantages of existing materials has attracted much research interest. By blending with PBS, which has better toughness and heat resistance, the disadvantages of PLA in terms of brittleness, low melt strength, and poor thermal stability can be avoided.

3. Blending modification of PLA to improve the performance of printed parts

The process of modification by blending PBS with PLA is shown in **Figure 2**. The dried PBS and PLA pellets were premixed and added to the twin-screw extruder for melt blending, and the specific formulations are listed in **Table 2**. The obtained blends were pelletized and extruded as 1.75 ± 0.02 mm filaments by a single-screw extruder for FDM 3D printing. This section provides a reference for determining

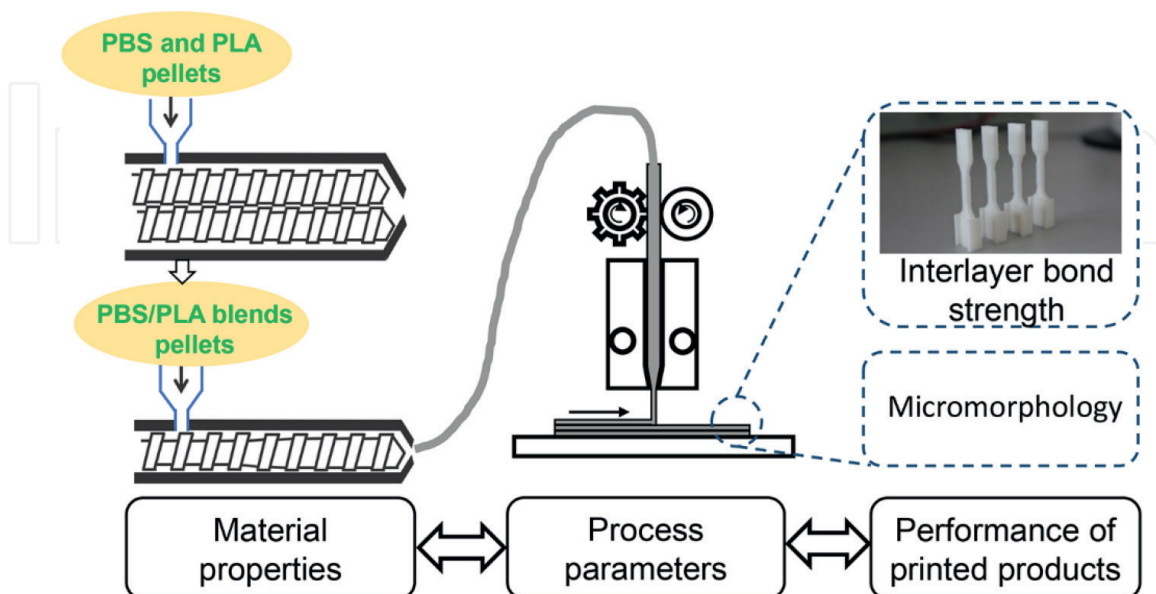


Figure 2. Schematic diagram of the process of blending PBS and PLA, extrusion of filaments, and FDM 3D printing using the blend filaments.

Sample	Content (wt%)	
	PBS	PLA
PBS100	100	0
PBS80/PLA20	80	20
PBS60/PLA40	60	40
PBS40/PLA60	40	60
PBS20/PLA80	20	80

Table 2.
 Sample information of PLA/PBS blends.

whether a thermoplastic polymer is suitable for FDM printing by studying the relationship between the rheological and crystallization properties of the PBS/PLA blends, process parameters, and the performance of the printed products [20].

3.1 Characterization of PBS/PLA blends

3.1.1 Rheological properties of the blends

The viscosity of the filament affects the FDM printing process. It has been reported that the modulus/viscosity ratio of the filament before entering the heating zone should be in the range of $(3-5) \times 10^5 \text{ s}^{-1}$ to ensure continuous and stable conveying without bending near the feed pinch rollers [21]. If the filament melt viscosity is too high, it can lead to extrusion difficulties, affecting the performance of the printed part or even leading to print failure. Therefore, the proper melt viscosity is also critical for filament FDM printing. The modified blends were subjected to a rotational rheology test to investigate the rheological properties, and the results are shown in **Figure 3**. The zero-shear viscosity of the blends gradually decreased with the increase in PBS content. And the Newtonian plateau area widens and the shear thinning effect weakens at 60% PBS content and above. This is because the zero-shear viscosity of PLA is much higher than that of PBS at the test temperature. **Figure 3b** and **c** shows the storage modulus (G') and loss modulus (G'') of the blends. Similarly, since the modulus of PLA is higher than that of PBS, the modulus of the blends gradually decreases with the increase in PBS content.

The FDM-3D printing process is accompanied by the cooling and solidification of the material, so it is necessary to study the thermal properties of the raw material. The crystallinity of the PBS/PLA blends increases with the PBS content, as shown in **Figure 4a**. Since the PLA used here is nearly amorphous, the apparent crystallinity in the blends decreases with the addition of PLA. The mechanical properties of the PBS/PLA blend bars produced by injection molding using a microinjection molding machine are shown in **Figure 4b** and **c**. The tensile strength and modulus of the blends had no significant changes when the PBS content was below 40%. However, when the PBS content continued to increase, the tensile modulus decreased sharply while the tensile strength decreased slightly. Elongation at break of blends increased with increasing PBS content, reaching a maximum of 356% at a PBS content of 80%. This was attributed to the effect of lower content of PLA as a rigid filler on the toughening of the blends.

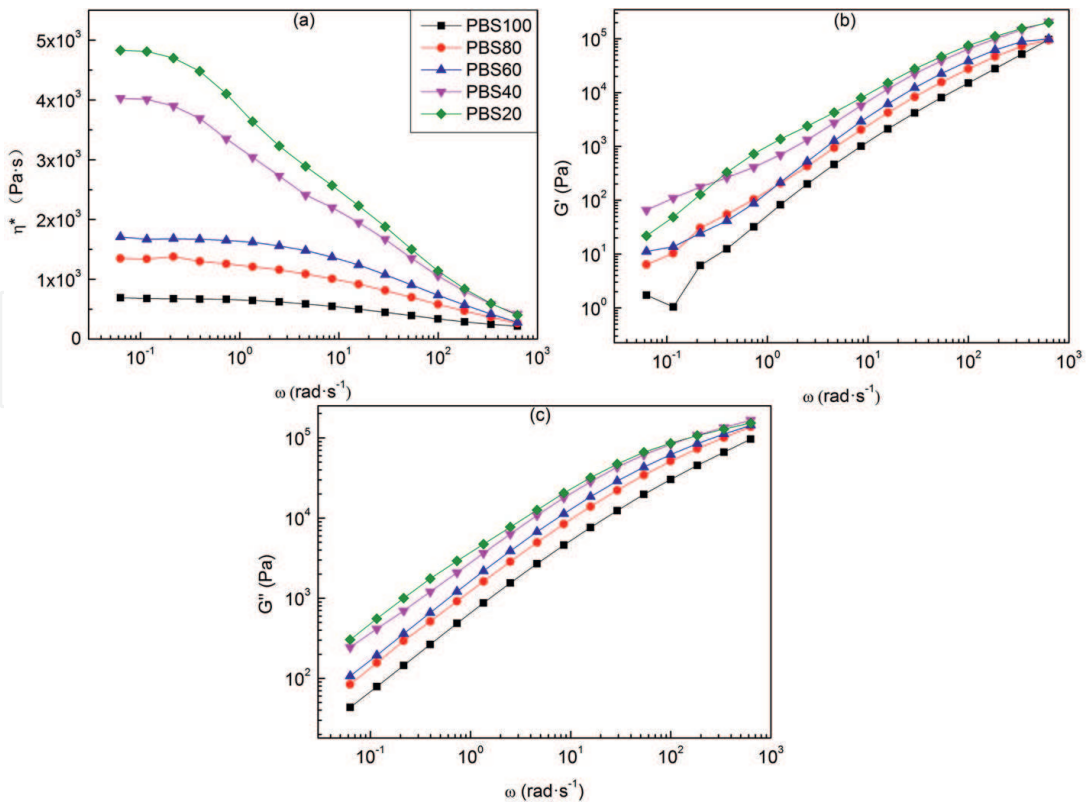


Figure 3. (a) Plots of the complex viscosity (η^*), (b) storage modulus (G'), and (c) loss of crystalline and mechanical properties of the blends. (a–c) Reproduced under the terms of the CC-BY Creative Commons Attribution 4.0 International license (<https://creativecommons.org/licenses/by/4.0/>) [20]. Copyright 2018, The Authors, published by American Chemical Society.

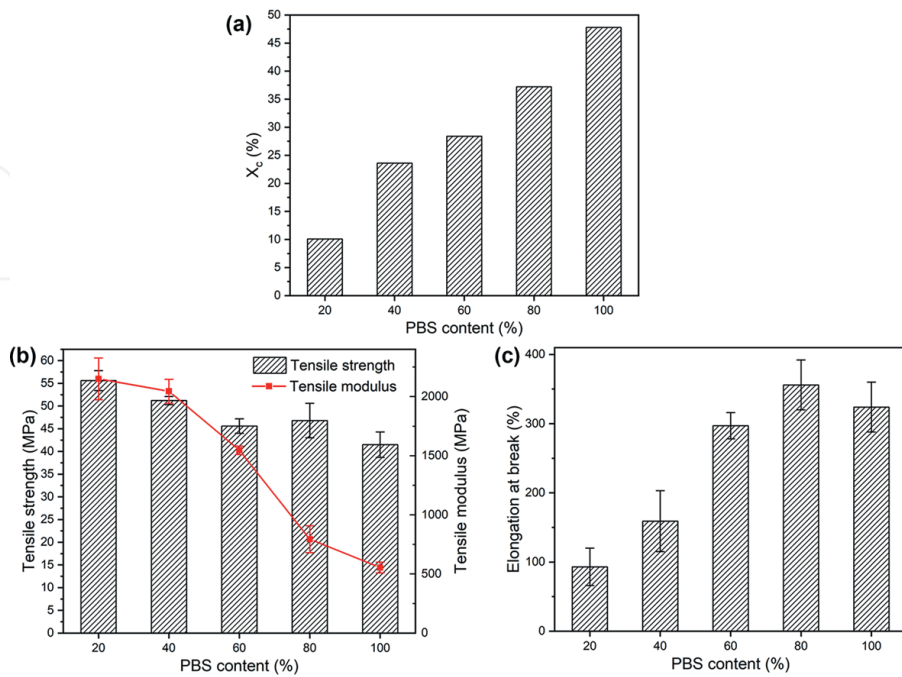


Figure 4. (a) Crystallinity of PBS/PLA blends, (b) Tensile strength, modulus, and (c) elongation at break of the PBS/PLA blend bars produced by injection molding.

3.2 Performance characterization of PBS/PLA blends for printed parts

Filaments of different blends were used to print different specimens and models with an FDM printer (AOD Dreamer, Qingdao Autolay 3D printing Co., Ltd. China). The printing parameters are listed in **Table 3**. In particular, all tests were printed with the platform unheated.

Preprinting experiments were first performed, that is, the appearance of the printed bars as well as the cross-sectional morphology were characterized. As shown in **Figure 5**, the dimensional stability of the PBS/PLA blended bars was good at low PBS content, and a significant warpage deformation was observed at PBS content higher than 60%. Combined with **Figure 4a** and **b**, it can be seen that this is because the crystallinity of the blends increased and the modulus decreased as the PBS content increased. Therefore, the print bars generated a large thermal stress gradient during the layer-by-layer deposition process leading to an increase in volume shrinkage, which resulted in severe warpage. The warpage deformation is very detrimental to the FDM 3D printing process, especially for large-area products, which may lead to print failure owing to the detachment of the printed part from the platform. Therefore, the low crystallinity, as well as a high modulus of the raw material, is essential when choosing a printing material.

Process parameters	
Nozzle diameter	0.4 mm
Nozzle temperature	190°C
Printing speed	1.5 m/min
Layer height	0.1 mm
Raster angle	+ 45° / - 45°
Infill ratio	100%

Table 3.
Printing parameters of PBS/PLA blend filament.

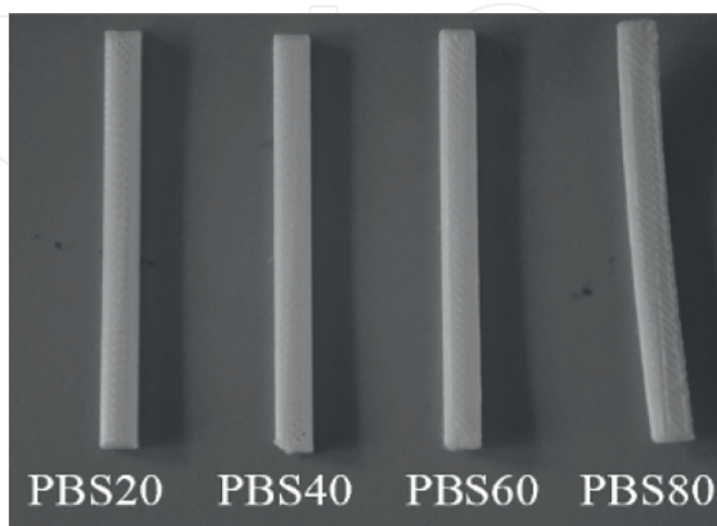


Figure 5.
Appearance of the PBS/PLA blend bars prepared by FDM printing. Reproduced under the terms of the CC-BY Creative Commons Attribution 4.0 International license (<https://creativecommons.org/licenses/by/4.0/>) [20]. Copyright 2018, The Authors, published by American Chemical Society.

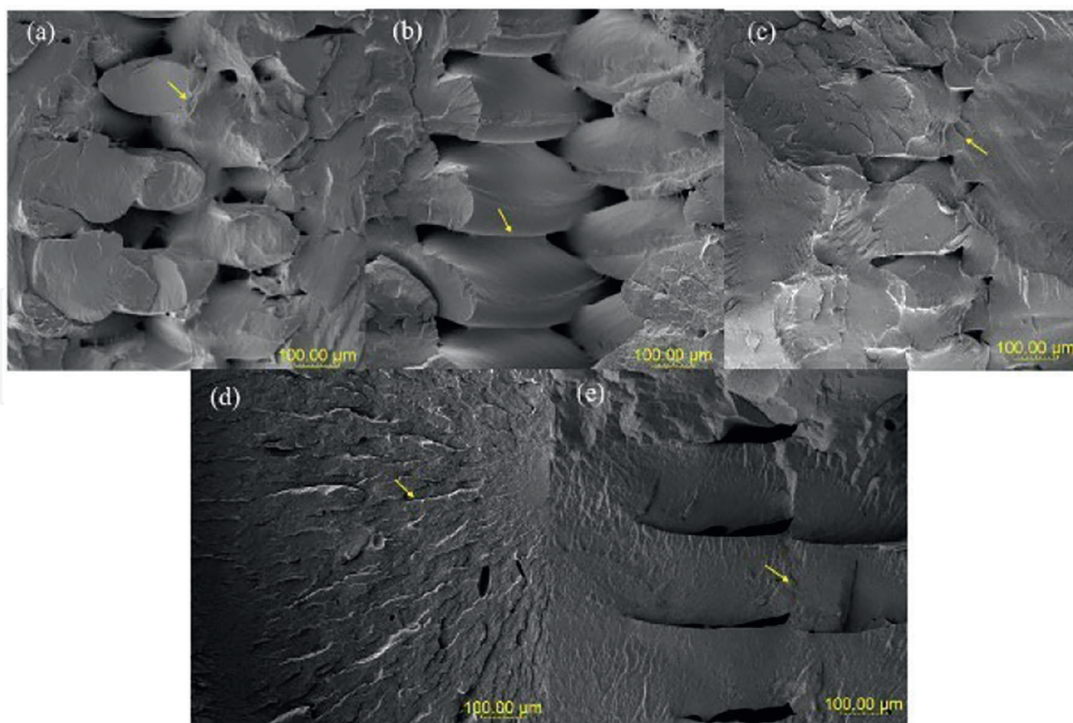


Figure 6.

SEM images of cross sections of the FDM-printed bars. (a) PBS20/PLA80, (b) PBS40/PLA60, (c) PBS60/PLA40, (d) PBS80/PLA20, and (e) PBS100. (a–e) Reproduced under the terms of the CC-BY Creative Commons Attribution 4.0 International license (<https://creativecommons.org/licenses/by/4.0/>) [20]. Copyright 2018, The Authors, published by American Chemical Society.

SEM images of cross sections of the FDM-printed bars are shown in **Figure 6**. The cross-sectional morphology after brittle fracture by liquid nitrogen shows that there are more obvious pores between the layers as well as the filaments at lower PBS content. The interlayer interface was gradually blurred when the PBS content was higher than 60%. This is owing to the lower viscosity and better flowability of the blends at higher PBS content (**Figure 2a**), which results in better interlayer interface bonding. PBS40/PBS60 was selected for the subsequent study considering the appearance, cross-section of the printed bars, the crystallization, and rheological properties of the blends.

From the above results, it can be inferred that the bonding of the interlayer interface is closely related to the viscosity of the melt. The main factor affecting the melt viscosity is the temperature. Therefore, the effect of temperature on the melt viscosity of the blends was further investigated. **Figure 7** shows the zero-shear viscosity of the PBS40/PLA60 blends at different temperatures. The zero-shear viscosity of the blend melt was below 1000 Pa·s and no longer decreased significantly above 190°C. The melt viscosity increased sharply when the temperature decreased from 190 to 160°C, which is detrimental to the printing process. Higher melt viscosity may clog the nozzle and cause underfilling, thus affecting the performance of the printed part. Therefore, the optimal printing temperature range is 190–230°C.

After determining the printing temperature window, the interlayer bond strength of the blends was further investigated at different printing temperatures. **Table 4** shows the tensile strength of the vertically printed samples at different printing temperatures and the melt viscosity of the corresponding blends. The interlayer bond strength decreased with PBS content at the same printing temperature. This is attributed to the increase in melt viscosity with increasing PLA content, which leads to the formation of larger interfilament gaps, resulting in a decrease in bond strength. For the PBS40/

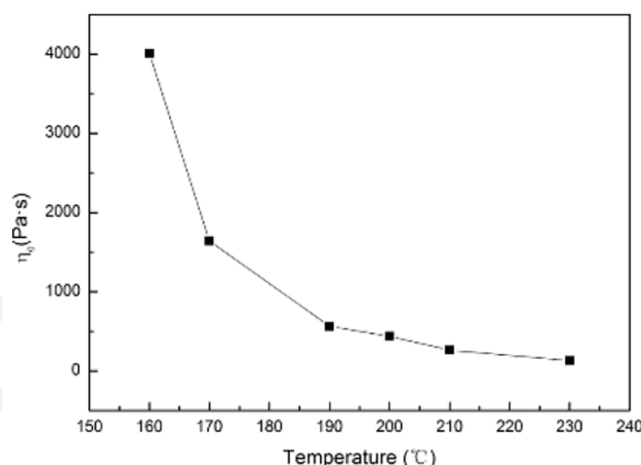


Figure 7. Variation of the zero-shear viscosity of PBS₄₀/PLA₆₀ melt with temperature. Reproduced under the terms of the CC-BY Creative Commons Attribution 4.0 International license (<https://creativecommons.org/licenses/by/4.0/>) [20]. Copyright 2018, The Authors, published by American Chemical Society.

Blends	Printing temperature (°C)	Zero-shear viscosity (Pa·s)	Tensile strength (MPa)
PBS100	210	67	25.0 ± 1.2
PBS80/PLA20	210	96	20.5 ± 1.3
PBS60/PLA40	210	123	19.6 ± 1.1
PBS40/PLA60	190	564	21.4 ± 5.2
PBS40/PLA60	200	438	19.5 ± 2.7
PBS40/PLA60	210	262	18.4 ± 2.7
PBS40/PLA60	230	130	16.5 ± 2.7

Reproduced under the terms of the CC-BY Creative Commons Attribution 4.0 International license (<https://creativecommons.org/licenses/by/4.0/>) [20]. Copyright 2018, The Authors, published by American Chemical Society.

Table 4. Interlayer bond strengths of the bars printed from different blend filaments or at different nozzle temperatures.

PLA₆₀ blend, the melt viscosity gradually decreased as the printing temperature increased from 190 to 230°C, and the interlayer adhesion strength gradually decreased. Generally, the decrease in melt viscosity at an increasing temperature is beneficial to interlayer bonding. The PLA used here is amorphous and has low crystallinity. It is presumed that the reduction of interlayer bonding may be due to the thermal degradation of PLA at higher than 190°C. Therefore, for printing materials, it is important to understand the relationship between material properties, processing, and performance of printed products, which helps to determine the appropriate printing process and thus obtain the optimal print product performance.

FDM 3D printing usually requires polymer materials with moderate melt viscosity, a certain tensile strength and toughness, low coefficient of thermal expansion, and good adhesion properties, as shown in **Figure 8**. From the point of view of polymer properties, it is necessary to select polymer materials that are suitable for the printing conditions. In practice, it is the melt viscosity, volumetric shrinkage, warpage, modulus, strength, interlayer bonding, and other properties of raw materials and the printed product that determine whether the material can be used in 3D printing.

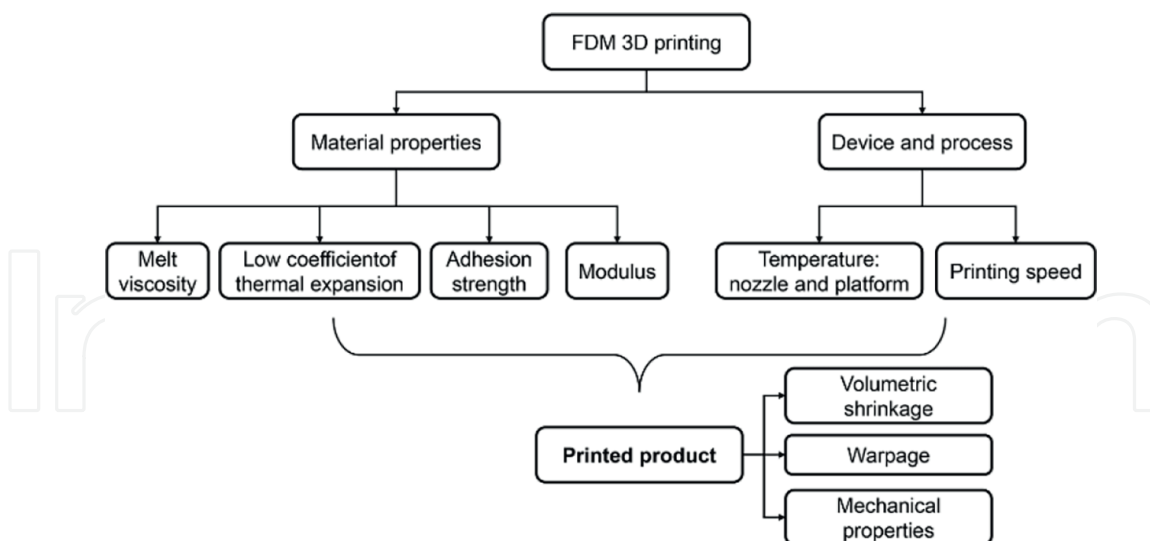


Figure 8.
Factors influencing the performance of FDM 3D printed products.

In addition, process parameters, such as nozzle temperature, platform temperature, printing speed, infill density, etc. are also important.

4. Pellet extrusion 3D printer based on micro-screw

Among biodegradable polymers, polyhydroxyalkanoates (PHAs) have attracted significant attention as a promising new family of sustainable polymers that are biobased and biodegradable in natural environments, with adjustable mechanical and physical properties [22]. PHAs are stable with respect to moisture and air exposure as they require an active microbial environment for degradation. Among various PHAs, the most common one, polyhydroxybutyrate (PHB), is brittle and hard. To solve the shortcomings, it can be copolymerized with an appropriate amount of 3-hydroxyvaleric acid (HV) monomers to improve the toughness. The melting point of the corresponding copolymer decreases with increasing HV fraction. Unlike polyolefins, some PHA melts have low thermal stability. Studies have shown that the molecular weight of PHAs may decrease during processing due to random chain scission [23].

PHA has a relatively high crystallinity like conventional polymers, such as polyethylene (PE) and polypropylene (PP). However, compared with commercial thermoplastic materials, it also has disadvantages such as higher cost and narrow processing window. Many studies have been conducted to modify product properties by blending PHA with PLA, improving its mechanical strength and customizable biodegradability [24, 25]. Wood is a natural organic material widely used in the form of sawdust, ground into smaller parts, or fine wood flour (WF) [19, 26]. Through the melt blending of WF and PHA, costs are reduced. In addition, the presence of wood filler can provide nucleation sites to promote rapid polymer crystallization from the melt, overcoming the slow crystallization of PHAs, which is a marked limitation for practical applications [23].

However, difficulties in preparing the filament and the feed section of biodegradable composites [27, 28] have limited the application of FDM for filament extrusion. Despite these difficulties, the inherent anisotropy of crystalline biodegradable composites can lead to a warpage of the printed part and thus prevent the print from

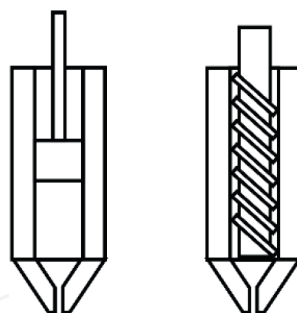


Figure 9.
Diagram of plunger and screw extrusion nozzles in FDM.

being completed. Therefore, FDM technology must be combined with traditional manufacturing techniques. FDM-based technology has developed two main types of structured print nozzles. As shown in **Figure 9**, one incorporates a screw nozzle design and the other a plunger nozzle. The screw nozzle is commonly used for industrial and biomedical printing applications, while the plunger is commonly used for applications such as food or clay printing.

In the case of plunger extrusion FDM technology, during the extrusion process, formulated “ink” are loaded into a cylinder (extruder) and the force generated by the hydraulic piston extrudes the “ink.” Successive layers are deposited by guiding the cylinder to a specific point on a predetermined three-dimensional model. However, plunger extruders cannot print continuously due to the limited volume within the cylinder. Previous studies [26, 29, 30] have also shown that the deposited products suffer from underfilling and poor accuracy, so plunger extrusion cannot be used for fused deposition molding of biomass composites.

Therefore, this section describes a micro-screw extrusion AM system suitable for the printing of fully biodegradable composites [31]. Specifically, it covers the design of micro-screws for different types of materials (crystalline and noncrystalline materials), the preparation of wood flour-filled polyhydroxyalkanoate (PHA) composites, and the elaboration of the relationship between materials properties, device design, and printed part performance [32].

Figure 10 shows the process diagram for micro-screw-based FDM 3D printing of WF/PHA composites. The dried PHA pellets were premixed with WF in the proportions listed in **Table 5** and then extruded in a twin-screw extruder in melt blending. The obtained WF/PHA composite pellets are pulverized and used directly for printing on a micro-screw 3D printer. The relationship between material properties, equipment and process parameters, and printed product performance was investigated. Combining traditional processing techniques with 3D printing increased the variety of printable materials and the depth of processing, thus providing a reference for the development of new 3D printing materials and equipment.

4.1 Micro-screw extrusion-based FDM system

A schematic diagram of the proposed micro-screw extrusion FDM 3D printer is shown in **Figure 10**, which consists of a micro-screw extrusion system, motion system, and control system. The fully biodegradable composite was extruded into a 0.1–3 mm filament by a micro-screw extrusion device and then deposited on the printing platform by an AM system based on FDM technology to realize layer-by-layer stacking and shaping.

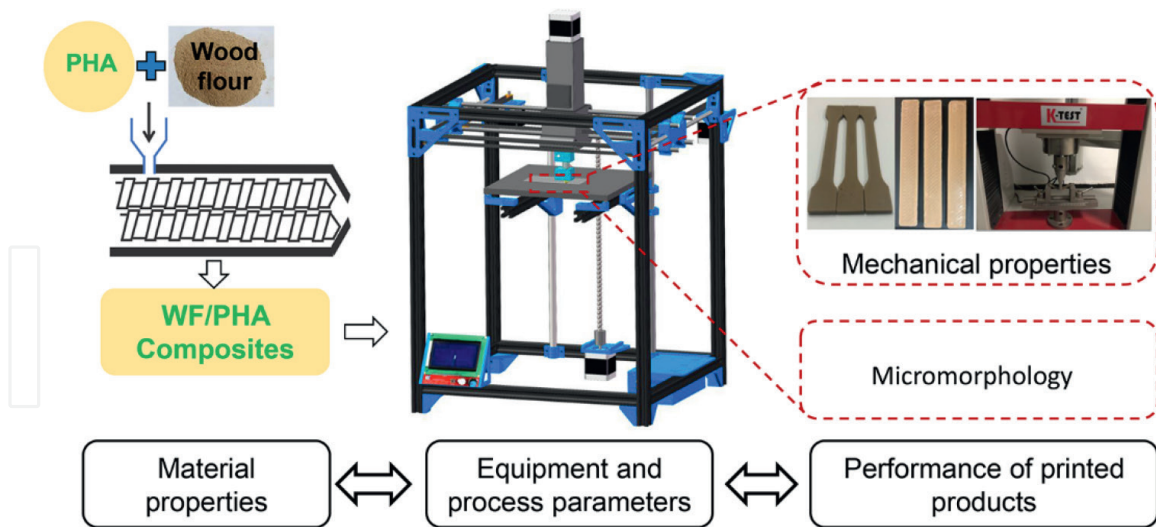


Figure 10. Process diagram for micro-screw-based FDM 3D printing of WF/PHA composites.

Sample	Content (wt%)	
	PHA	WF
10WF/PHA	90	10
20WF/PHA	80	20
30WF/PHA	70	30

Table 5. Parameters of WF/PHA composites.

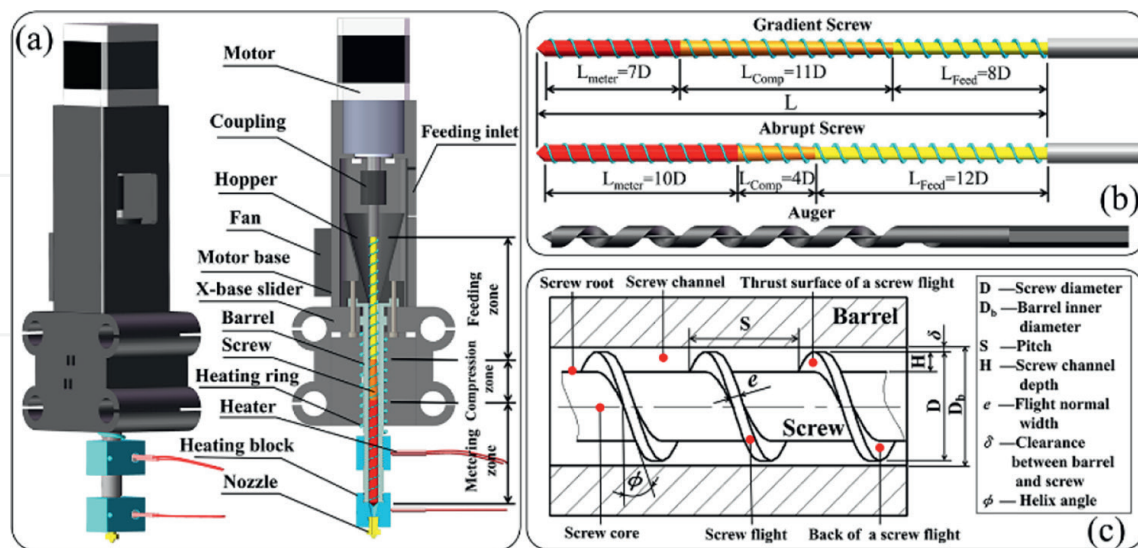


Figure 11. Micro-screw extrusion system. (a) 3D and cross-sectional views of the micro-screw extrusion system, (b) a schematic diagram of two types of screws and an auger, and (c) notations for screw geometry. (a-c) Adapted with permission [31]. Copyright 2021, Elsevier.

Figure 11a shows a three-dimensional view and cross-sectional view of the micro-screw extrusion system. The micro-screw extrusion system consists of a planetary reduction stepper motor, motor base, hopper, X-base slider, barrel, micro-screw,

heating block, and brass nozzle. The micro screw is driven by a stepper motor at one end and the other end penetrates the hopper into the barrel. The micro screw extrusion is, therefore, fed continuously and forcibly without feeding difficulties compared with filament extrusion. Three heating zones on the outside of the barrel allow the material to be completely molten. The micro-screw drives the material in the extrusion direction to obtain a stable extrusion pressure, which improves the melt plasticization quality and improves the performance of the 3D printed product. Overall, micro-screw extrusion 3D printing can achieve higher melting and printing efficiency than filament extrusion FDM 3D printing, resulting in continuous and stable printing. **Figure 11b** shows two types of screws designed according to the material properties and the 3D printing process, as well as the conveying-only auger used for comparison. For the conventional screw design, the gradient screw is suitable for amorphous polymer processing, while the abrupt screw is suitable for crystalline polymer. **Figure 11c** shows the specific parameters of the screw structure. In order to achieve excellent nozzle dynamics [33], a screw diameter of 6 mm, an L/D ratio of 26, and a compression ratio of 2.9 were designed. The ratios of the feeding, compression, and metering section lengths of the gradient screw and abrupt screw were 8D:11D:7D and 12D:4D:10D, respectively.

4.2 Rheological properties of WF/PHA composites

Investigating the rheological properties of raw materials prior to micro-screw extrusion 3D printing can help to optimize the printing process and thus improve the

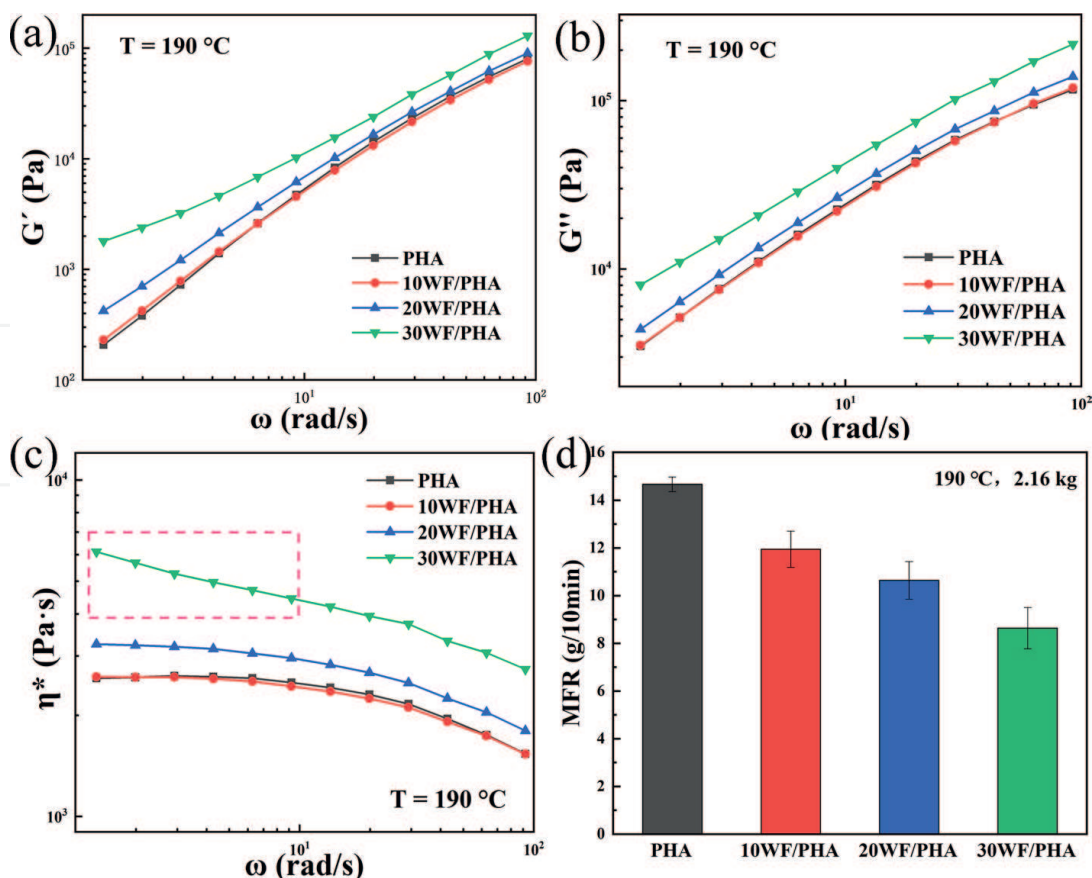


Figure 12. Rheological properties of neat PHA and WF/PHA composites: (a) storage modulus, (b) loss modulus, (c) complex viscosity, and (d) MFR. (a–d) Reproduced with permission [31]. Copyright 2021, Elsevier.

performance of the printed product. The properties of 3D printed materials require, on one hand, sufficient fluidity to ensure adequate bonding to the previous layer after deposition and, on the other hand, sufficient melt strength to ensure shape stability. **Figure 12** shows the rheological properties of neat PHA and WF/PHA composites. WF is often used as a filler to improve the dimensional stability, rigidity, and heat resistance of the matrix resin and is widely used in the processing of wood-plastic composites. As a result, the modulus of WF/PHA composites increased compared with neat PHA. Furthermore, **Figure 12a** and **b** shows that the loss modulus (G'') of neat PHA and the composite is higher than the storage modulus (G'), exhibiting typical viscoelastic properties. The complex viscosity (η^*) of the composites increased with the WF content, as shown in **Figure 12c**. Furthermore, the shear thinning effect of the composites was stronger with the increase in WF content, indicating an improved processing range of the composites. **Figure 12d** shows the MFR of the neat PHA and WF/PHA composites. The fluidity of the composites decreased with the increase in WF content. This is consistent with the results of viscosity in the rotational rheology test, where the increased WF content in the composite impedes the movement of the polymer chain segments, thus reducing fluidity.

4.3 Stability of extrusion flow rate and analysis of pressure-building capacity

The extrusion stability and pressure-building capability of screw extrusion 3D printers are closely related to screw design and composite rheological properties. **Figure 13a** and **b** presents extrusion stability curves of neat PHA and WF/PHA composites extruded at various nozzle temperatures and different screw speeds. The effect of screw speed on the extrusion output (Q) was more significant than the effect of temperature. At the same temperature, the Q of the WF/PHA composites decreased as the WF content increased, which is consistent with the rheological test results. For micro-screw extrusion, the Q of neat PHA was not sensitive to temperature. This indicates that the screw working characteristic was not suitable for neat PHA. The Q of WF/PHA composites was stable at 190°C and did not increase significantly at higher temperatures. The discontinuity defect shown in **Figure 13a** appeared above 200°C, which was caused by partial degradation of the WF at higher temperatures. The Q of WF/PHA composites was linearly related to the screw speed at the same temperature. This is essential for controlling Q by screw speed and thus regulating the performance of the printed product.

Figure 13c shows the melt pressure of neat PHA and WF/PHA composites with various WF contents at different screw speeds. The SEN-PT series of the miniature pressure sensor (accuracy $\pm 1\%$ FS, mounting thread size M14*1.5) was adopted to measure the melt pressure at different screw speeds. The melt pressure signal can be output *via* the accompanying digital display instrument and monitored online in real-time and recorded when the melt pressure data is stable. Because Q increased with increasing screw speed, the melt pressure of neat PHA and WF/PHA composites increased with increasing screw speed. The melt pressure of WF/PHA composites decreased with increasing WF content at the same screw speed. The determining factor for melt pressure is actually the amount of melt built-up in the nozzle chamber and is, therefore, related to Q . As Q decreased with increasing WF content, the corresponding melt pressure also decreased.

It is worth noting that the rheological characteristic curves of neat PHA and 10WF/PHA in **Figure 12a–c** largely overlap, but neat PHA is unable to complete printing due to warpage and underfilling (**Figure 13d**). This is because the addition

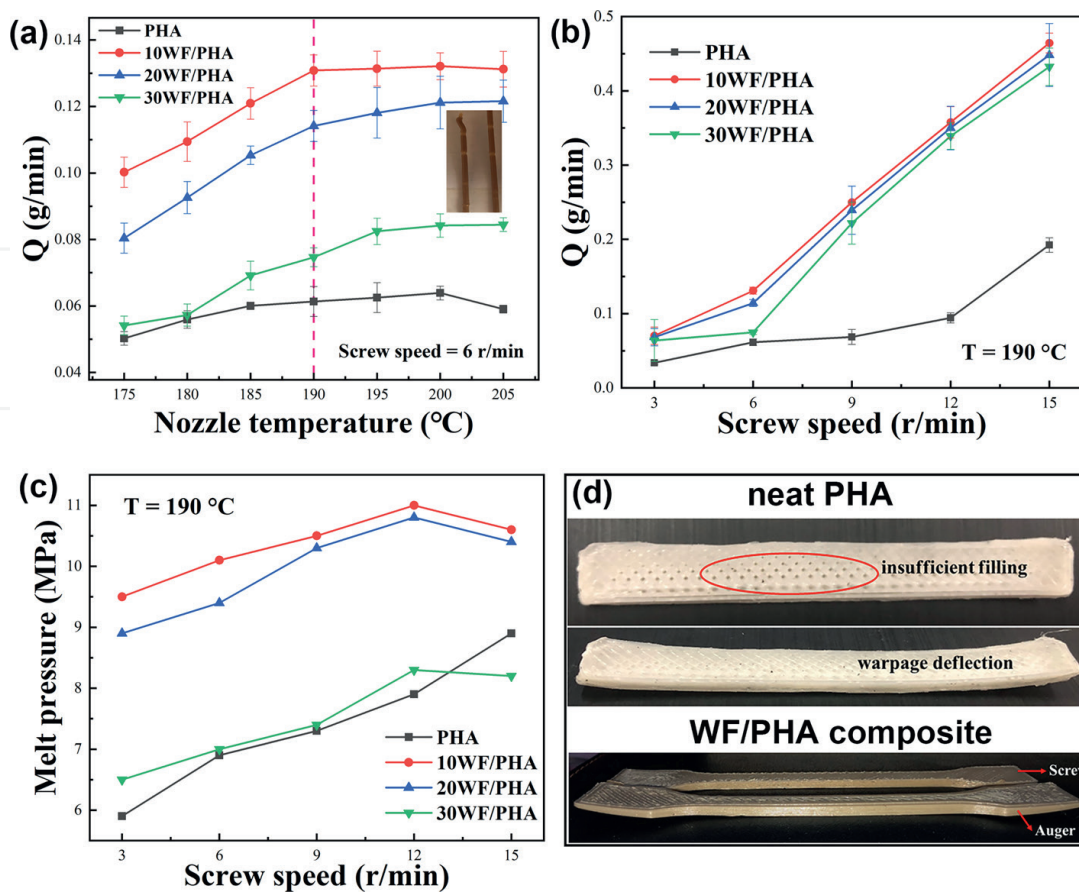


Figure 13. Extrusion stability curves of WF/PHA composites extruded at (a) various nozzle temperatures and (b) different screw speeds. (c) Melt pressure of neat PHA and WF/PHA composites with various WF content at different screw speeds. (d) Printing defects of neat PHA and WF/PHA composite samples printed by micro-screw and auger. (a–d) Reproduced with permission [31]. Copyright 2021, Elsevier.

of WF filler increased the modulus of the PHA as well as the Q. Moreover, the melt pressure curve also shows that the melt pressure of 10WF/PHA is much higher than that of neat PHA. Combined with the picture of the WF/PHA composite samples printed by micro-screw and auger under the same printing parameters in **Figure 13d**, the results show that the pressure-building capacity of the micro screw has a positive effect on the resistance to warpage.

4.4 Performance of micro-screw extrusion 3D printed WF/PHA composites

4.4.1 Effect of WF content and different raster angles on the mechanical properties of WF/PHA composite

As PHA is a semicrystalline material, an abrupt screw was used to investigate the effect of WF content and different raster angles on the mechanical properties of the product. The specific printing parameters were: nozzle temperature of 190°C, layer thickness of 0.3 mm, printing speed of 15 mm/s, nozzle diameter of 1 mm, and 100% fill percentage. As shown in **Figure 14**, the impact, tensile, and flexural strengths of the composite decreased with increasing WF content, while the modulus increased significantly. This is due to the increased stiffness of the WF/PHA composites caused by the addition of WF. Furthermore, the stress-strain curves of the composites

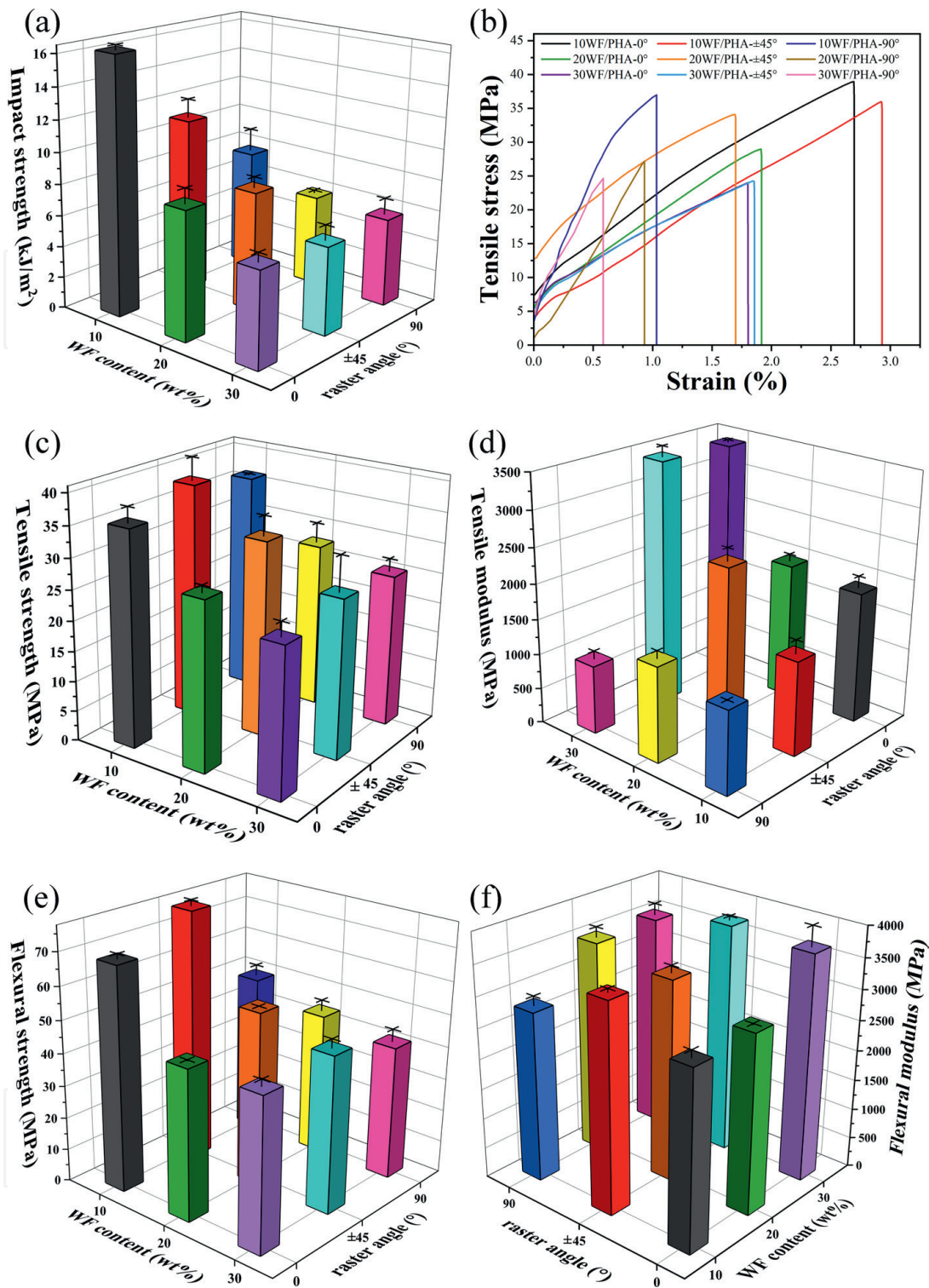


Figure 14. Mechanical properties of printed WF/PHA composites with various WF contents and different raster angles: (a) impact strength, (b) tensile stress-strain curves, (c) tensile strength, (d) tensile modulus, (e) flexural strength, and (f) flexural modulus. (a-f) Adapted with permission [31]. Copyright 2021, Elsevier.

exhibited typical brittle fracture, which can also be verified by the cross-sectional morphology of the composites in **Figure 15**. In addition, raster angles have a significant effect on the mechanical properties of the composite, with the 45°/−45° print direction having the best mechanical properties. As can be seen in **Figure 15**, this is due to the denser deposition of the products printed at 45°/−45° compared with 0°

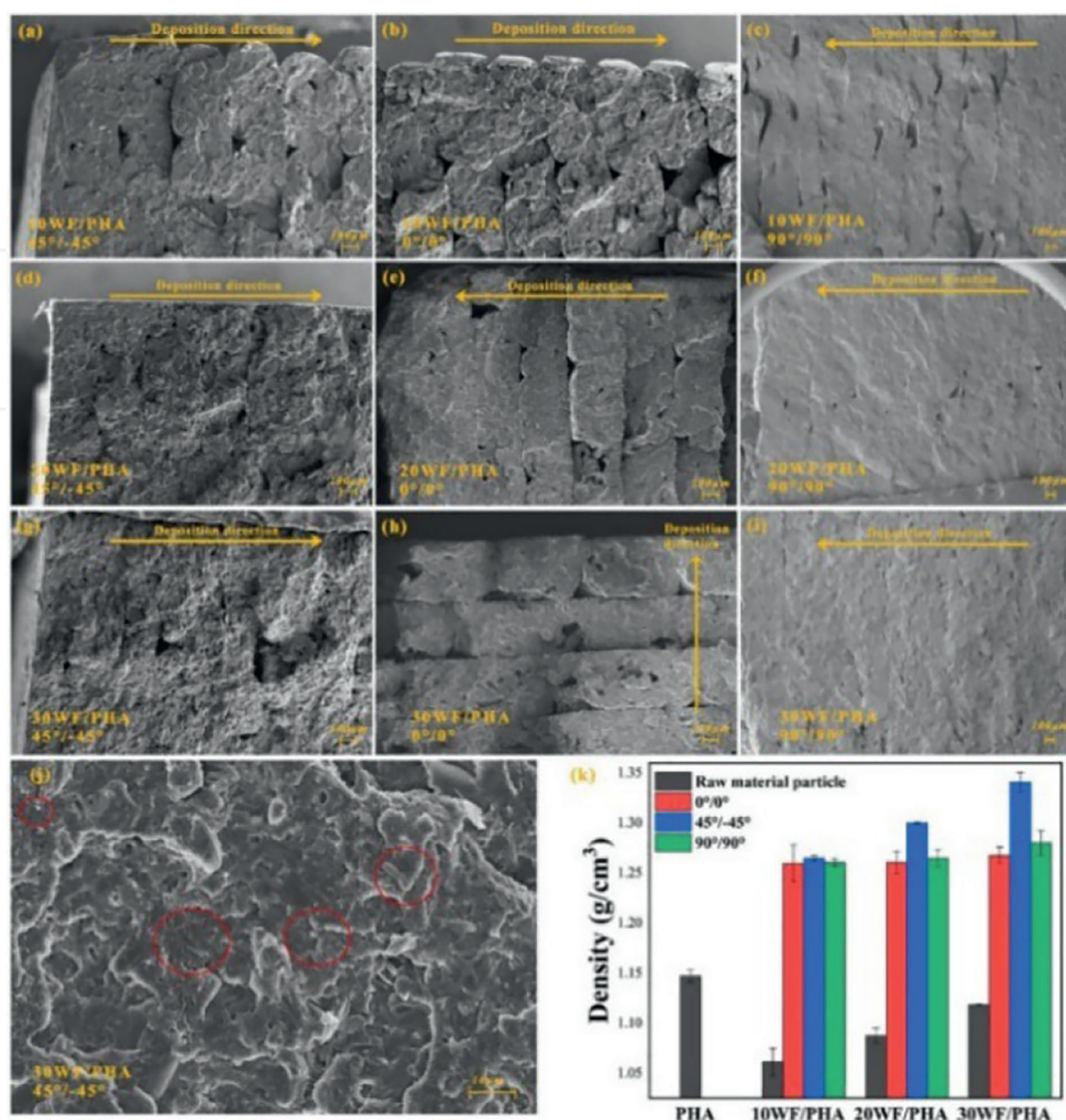


Figure 15. (a–j) SEM images of the fractured cross-section of WF/PHA composites, and (k) density of neat PHA and WF/PHA composites. (a–k) Reproduced with permission [31]. Copyright 2021, Elsevier.

and 90° raster angles, as verified by the fact that the WF/PHA printed at 45°/-45° has the highest density in **Figure 15k**. However, the difference in mechanical properties of the composites with different raster angles decreased with the increasing WF content. This further supports the role of WF in improving the printability of PHA and reducing anisotropy.

4.4.2 Effect of screw structure on the mechanical properties of WF/PHA composite

Screw structure influences the performance of the printed product mainly by affecting the plasticizing quality and the extrusion output. Therefore, the difference in Q between the two screws at different screw speeds was first compared and the results are shown in **Figure 16a**. The Q of the gradient screw was higher than that of the abrupt screw at screw speeds below 13 r/min. The difference between the two types of screws is mainly in the length of the three sections of the screw (**Figure 11b**), while the Q of the single screw depends on the metering section. The metering section of the gradient screw is shorter than that of the abrupt screw and conveys the melt

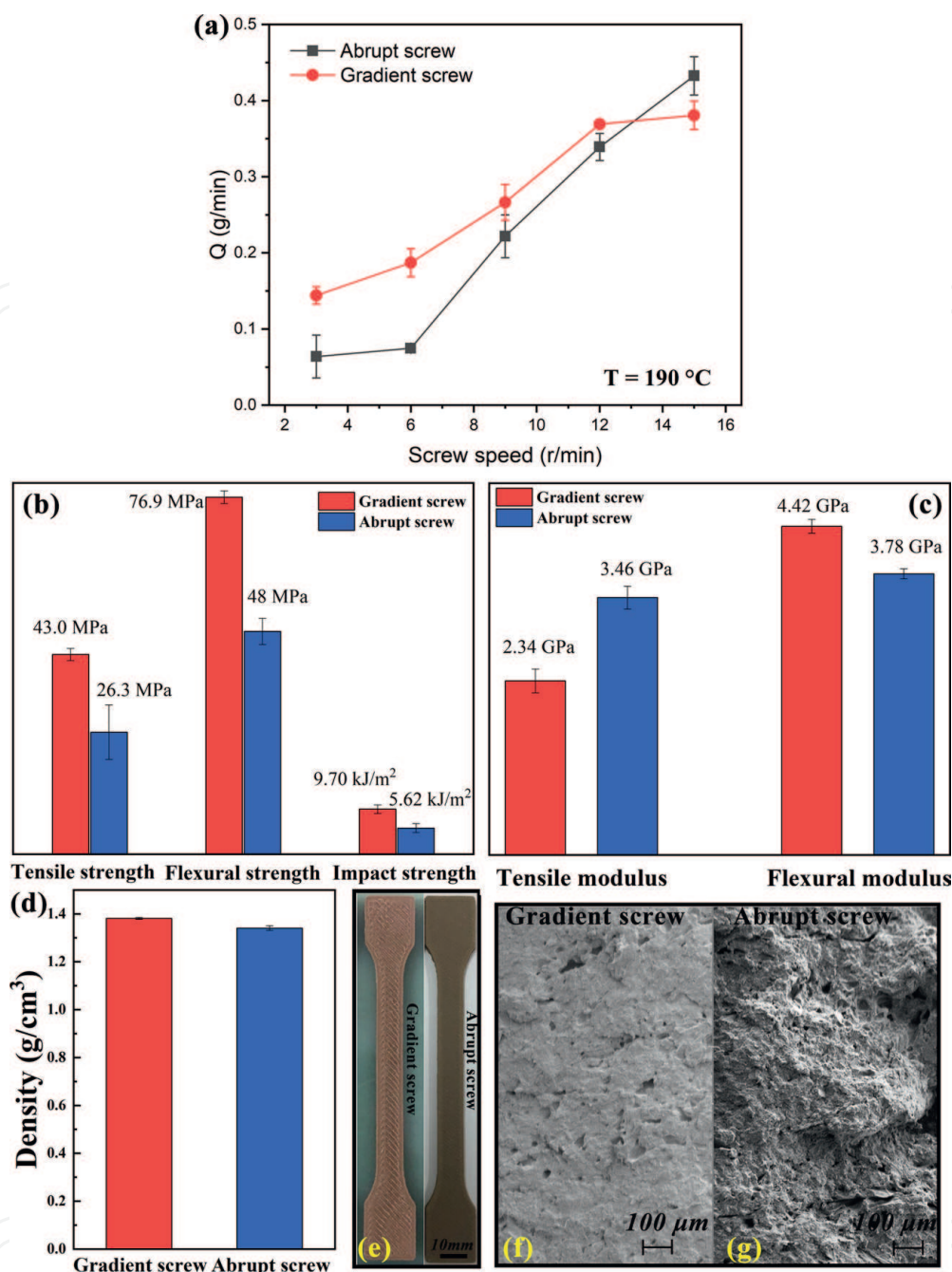


Figure 16. (a) Extrusion output for two screws at different screw speeds, (b) Mechanical strength, (c) modulus, (d) density, (e) surface quality, and (f–g) SEM images of samples printed by two kinds of screws. (b–g) Adapted under the terms of the CC-BY Creative Commons Attribution 4.0 International license (<https://creativecommons.org/licenses/by/4.0>) [32]. Copyright 2021, The Authors, published by MDPI.

much more efficiently, resulting in a higher Q for the gradient screw. The higher Q results in a denser sample build-up, so the mechanical properties of the bars printed by the gradient screw were higher than those printed by the abrupt screw. This can be verified in **Figure 16d–g**, where the gradient screw-printed samples were denser than those of the abrupt screw, and the sample surface was uneven due to over-extrusion, while the abrupt screw printed samples had more porosity in the cross-section. This can be verified in **Figure 16d–g**: the densities of the samples printed by the gradient screw are higher than those of the abrupt screw; the surfaces of the samples printed

by the gradient screw are uneven due to over-extrusion; and the cross-sections of the samples printed by the abrupt screw have more porosity.

The performance of micro-screw extrusion 3D-printed products is influenced in many ways by material properties, process conditions, and equipment parameters. Establishing a process-structure-performance relationship is, therefore, essential for choosing 3D printing material and design of equipment.

5. Conclusions

3D printing technology has shown rapid diversification in recent years and has unique advantages in the innovative manufacturing of customized products. To achieve the goal of green and sustainable economic development, combining 3D printing with biodegradable materials will not only broaden the range of methods for forming biodegradable products but also enrich the range of environment-friendly materials available for 3D printing.

In filament extrusion FDM, a promising biodegradable polymer blend PBS/PLA was formulated, which combined the advantages of high modulus and low warpage of PLA with the toughness of PBS. PBS60/PLA40 and PBS40/PLA60 blends have a better appearance, less warpage, and higher dimensional accuracy and can be used as an alternative to PLA for FDM 3D printing.

For pellet extrusion FDM, we have solved the problem that WF/PHA composites cannot be used in 3D printing owing to difficulties in filament extrusion by designing new 3D printing equipment. The micro-screw extrusion 3D printing device is characterized by wide material adaptability, high printing efficiency, and low cost. The printability of the composite material was evaluated by testing the extrusion flow rate stability and the pressure-building ability of the micro-screw extrusion device. The effects of material properties, equipment structure, and process parameters on the performance of printed products are explored. The process-structure-performance relationship of micro-screw extrusion 3D printing is further illustrated.

Searching for new biodegradable polymers that can be 3D printed is still in progress and will greatly widen the application of FDM-based 3D printing in both industry and our daily life.

IntechOpen

Author details


Jing Tian¹, Yanyan Zheng¹, Qing Ouyang¹, Ping Xue², Baohua Guo¹ and Jun Xu^{1*}

1 Department of Chemical Engineering, Tsinghua University, Beijing, China

2 Department of Mechanical and Electrical Engineering, Beijing University of Chemical Technology, Beijing, China

*Address all correspondence to: jun-xu@mail.tsinghua.edu.cn

IntechOpen

© 2023 The Author(s). Licensee IntechOpen. This chapter is distributed under the terms of the Creative Commons Attribution License (<http://creativecommons.org/licenses/by/3.0>), which permits unrestricted use, distribution, and reproduction in any medium, provided the original work is properly cited. 

References

- [1] Kakadellis S, Rosetto G. Achieving a circular bioeconomy for plastics. *Science*. 2021;**373**(6550):49-50. DOI: 10.1126/science.abj3476
- [2] Rosenboom JG, Langer R, Traverso G. Bioplastics for a circular economy. *Nature Reviews Materials*. 2022;**7**:117-137. DOI: 10.1038/s41578-021-00407-8
- [3] Zhai Y, Lados DA, LaGoy JL. Additive manufacturing: Making imagination the major limitation. *Journal of Metals*. 2014;**66**(5):808-816. DOI: 10.1007/s11837-014-0886-2
- [4] Casavola C, Cazzato A, Moramarco V, Pappalettere C. Orthotropic mechanical properties of fused deposition modelling parts described by classical laminate theory. *Materials and Design*. 2016;**90**:453-458. DOI: 10.1016/j.matdes.2015.11.009
- [5] Mohamed OA, Masood SH, Bhowmik JL. Optimization of fused deposition modeling process parameters: A review of current research and future prospects. *Advanced Manufacturing*. 2015;**3**:42-53. DOI: 10.1007/s40436-014-0097-7
- [6] Solomon IJ, Sevvel P, Gunasekaran J. A review on the various processing parameters in FDM. *Materials Today Proceedings*. 2020;**37**:509-514. DOI: 10.1016/j.matpr.2020.05.484
- [7] Kumar NP, Kumar SA, Sankar MS. Effect of process parameters on the mechanical behavior of FDM and DMLS build parts. *Materials Today Proceedings*. 2019;**22**:1443-1451. DOI: 10.1016/j.matpr.2020.01.502
- [8] Rajpurohit SR, Dave HK. Effect of process parameters on tensile strength of FDM printed PLA part. *Rapid Prototyping Journal*. 2018;**24**:1317-1324. DOI: 10.1108/RPJ-06-2017-0134
- [9] Huang B, Meng S, He H, Jia Y, et al. Study of processing parameters in fused deposition modeling based on mechanical properties of acrylonitrile-butadiene-styrene filament. *Polymer Engineering and Science*. 2019;**59**:120-128. DOI: 10.1002/pen.24875
- [10] Benali N, Hammami D, Khlif M, Bradai C. Optimization of FDM manufacturing parameters of a biodegradable thermoplastic (PLA). In: *Proceedings of the Design and Modeling of Mechanical Systems - IV. CMSM 2019. Lecture Notes in Mechanical Engineering*; 18-20 March 2019; Hammamet. Tunisia: Springer, Cham; 2020. pp. 355-362
- [11] Chacón JM, Caminero MA, García-Plaza E, Núñez PJ. Additive manufacturing of PLA structures using fused deposition modelling: Effect of process parameters on mechanical properties and their optimal selection. *Materials and Design*. 2017;**124**:143-157. DOI: 10.1016/j.matdes.2017.03.065
- [12] Wang P, Zou B, Xiao H, et al. Effects of printing parameters of fused deposition modeling on mechanical properties, surface quality, and microstructure of PEEK. *Journal of Materials Processing Technology*. 2019;**271**:62-74. DOI: 10.1016/j.jmatprotec.2019.03.016
- [13] Dizon JRC, Espera AH, Chen Q, et al. Mechanical characterization of 3D-printed polymers. *Additive Manufacturing*. 2018;**20**:44-67. DOI: 10.1016/j.addma.2017.12.002
- [14] Ahn SH, Montero M, Odell D, Roundy S, Wright PK. Anisotropic

material properties of fused deposition modeling ABS. *Rapid Prototyping Journal*. 2002;**8**:248-257. DOI: 10.1108/13552540210441166

[15] Chaudhry MS, Czekanski A. Evaluating FDM process parameter sensitive mechanical performance of elastomers at various strain rates of loading. *Materials (Basel)*. 2020;**13**:1-10. DOI: 10.3390/ma13143202

[16] Zaldivar RJ, Witkin DB, McLouth T, et al. Influence of processing and orientation print effects on the mechanical and thermal behavior of 3D-Printed ULTEM ® 9085 material. *Additive Manufacturing*. 2017;**13**:71-80. DOI: 10.1016/j.addma.2016.11.007

[17] Hanon MM, Marczis R, Zsidai L. Influence of the 3D printing process settings on tensile strength of PLA and HT-PLA. *Period Polytechnical and Mechanical Engineering*. 2020;**65**:38-46. DOI: 10.3311/ppme.13683

[18] Guessasma S, Belhabib S, Nouri H. Microstructure and mechanical performance of 3D printed wood-PLA/PHA using fused deposition modelling: Effect of printing temperature. *Polymers (Basel)*. 2019;**11**:1778. DOI: 10.3390/polym11111778

[19] Chan CM, Vandi LJ, Pratt S, et al. Composites of wood and biodegradable thermoplastics: A review. *Polymer Reviews*. 2018;**58**(3):444-494. DOI: 10.1080/15583724.2017.1380039

[20] Ou-Yang Q, Guo B, Xu J. Preparation and characterization of poly(butylene succinate)/Polylactide blends for fused deposition Modeling 3D printing. *ACS. Omega*. 2018;**3**(10):14309-14317. DOI: 10.1021/acsomega.8b02549

[21] Venkataraman N, Rangarajan S, Matthewson MJ, et al. Feedstock material

property-process relationships in fused deposition of ceramics (FDC). *Rapid Prototyping Journal*. 2000;**6**:244-253. DOI: 10.1108/13552540010373344

[22] Vandi LJ, Chan CM, Werker A, et al. Wood-PHA composites: Mapping opportunities. *Polymers (Basel)*. 2018;**10**:751. DOI: 10.3390/polym10070751

[23] Reinsch VE, Kelley SS. Crystallization of poly(hydroxybutyrate-co-hydroxyvalerate) in wood fiber-reinforced composites. *Journal of Applied Polymer Science*. 1997;**64**(9):1785-1796. DOI: 10.1002/(SICI)1097-4628(19970531)64:9<1785

[24] Gonzalez Ausejo J, Rydz J, Musioł M, Sikorska W, Janeczek H, Sobota M, et al. Three-dimensional printing of PLA and PLA/PHA dumbbell-shaped specimens of crisscross and transverse patterns as promising materials in emerging application areas: Prediction study. *Polymer Degradation and Stability*. 2018;**156**:100-110. DOI: 10.1016/j.polymdegradstab. 2018.08.008

[25] Gerard T, Budtova T. Morphology and molten-state rheology of polylactide and polyhydroxyalkanoate blends. *European Polymer Journal*. 2012;**48**(6):1110-1117. DOI: 10.1016/j.eurpolymj.2012.03.015

[26] Kariz M, Sernek M, Kuzman MK. Use of wood powder and adhesive as a mixture for 3D printing. *European Journal of Wood Product*. 2016;**74**(1):123-126. DOI: 10.1007/s00107-015-0987-9

[27] Kariz M, Sernek M, Obućina M, Kuzman MK. Effect of wood content in FDM filament on properties of 3D printed parts. *Materials Today Communication*. 2018;**14**:135-140. DOI: 10.1016/j.mtcomm.2017.12.016

[28] Mazzanti V, Malagutti L, Mollica F. FDM 3D printing of polymers containing

natural fillers: A review of their mechanical properties. *Polymers (Basel)*. 2019;**11**:1094. DOI: 10.3390/polym11071094

[29] Godoi FC, Prakash S, Bhandari BR. 3d printing technologies applied for food design: Status and prospects. *Journal of Food Engineering*. 2016;**179**:44-54. DOI: 10.1016/j.jfoodeng.2016.01.025

[30] Lanaro M, Forrestal DP, Scheurer S, et al. 3D printing complex chocolate objects: Platform design, optimization and evaluation. *Journal of Food Engineering*. 2017;**215**:13-22. DOI: 10.1016/j.jfoodeng.2017.06.029

[31] Tian J, Zhang R, Wu Y, et al. Additive manufacturing of wood flour/polyhydroxyalkanoates (PHA) fully bio-based composites based on micro-screw extrusion system. *Materials and Design*. 2021;**199**:109418. DOI: 10.1016/j.matdes.2020.109418

[32] Tian J, Zhang R, Yang J, et al. Additive manufacturing of wood flour/PHA composites using Micro-screw extrusion: Effect of device and process parameters on performance. *Polymers (Basel)*. 2021;**13**(7):1107. DOI: 10.3390/polym13071107

[33] Yan Y, Li S, Zhang R, et al. Rapid prototyping and manufacturing technology: Principle, representative technics, applications, and development trends. *Tsinghua Science and Technology*. 2009;**14**:1-12. DOI: 10.1016/S1007-0214(09)70001-X